HHS Public Access

Author manuscript

ACS Nano. Author manuscript; available in PMC 2019 October 24.

Published in final edited form as:

ACS Nano. 2017 September 26; 11(9): 9223–9230. doi:10.1021/acsnano.7b04348.

Locally Induced Adipose Tissue Browning by Microneedle Patch for Obesity Treatment

Yuqi Zhang[†,‡,#], **Qiongming Liu**[§,#], **Jicheng Yu**[†,‡], **Shuangjiang Yu**[†,‖], **Jinqiang Wang**[†], **Li Qiang**[*,§], **Zhen Gu**[*,†,‡,⊥]

[†]Joint Department of Biomedical Engineering, University of North Carolina at Chapel Hill and North Carolina State University, Raleigh, North Carolina 27695, United States

[‡]Center for Nanotechnology in Drug Delivery and Division of Molecular Pharmaceutics, UNC Eshelman School of Pharmacy, University of North Carolina at Chapel Hill, Chapel Hill, North Carolina 27599, United States

[§]Department of Pathology and Cell Biology, Naomi Berrie Diabetes Center, Columbia University, New York, New York 10032, United States

[‖]Key Laboratory of Polymer Ecomaterials, Changchun Institute of Applied Chemistry, Chinese Academy of Sciences, Changchun, Jilin 130022, China

[⊥]Department of Medicine, University of North Carolina at Chapel Hill, Chapel Hill, North Carolina 27599, United States

Abstract

Obesity is one of the most serious public health problems in the 21st century that may lead to many comorbidities such as type-2 diabetes, cardiovascular diseases, and cancer. Current treatments toward obesity including diet, physical exercise, pharmacological therapy, as well as surgeries are always associated with low effectiveness or undesired systematical side effects. In order to enhance treatment efficiency with minimized side effects, we developed a transcutaneous browning agent patch to locally induce adipose tissue transformation. This microneedle-based patch can effectively deliver browning agents to the subcutaneous adipocytes in a sustained manner and switch on the “browning” at the targeted region. It is demonstrated that this patch reduces treated fat pad size, increases whole body energy expenditure, and improves type-2 diabetes *in vivo* in a diet-induced obesity mouse model.

Graphical Abstract

[*]**Corresponding Authors:** lq2123@cumc.columbia.edu. zgu@email.unc.edu.

[#]Y.Z. and Q.L. contributed equally.

Supporting Information

The Supporting Information is available free of charge on the ACS Publications website at DOI: 10.1021/acsnano.7b04348.

Supporting experimental section, Table S1, and Figures S1−S6 as noted in the text (PDF)

The authors declare no competing financial interest.

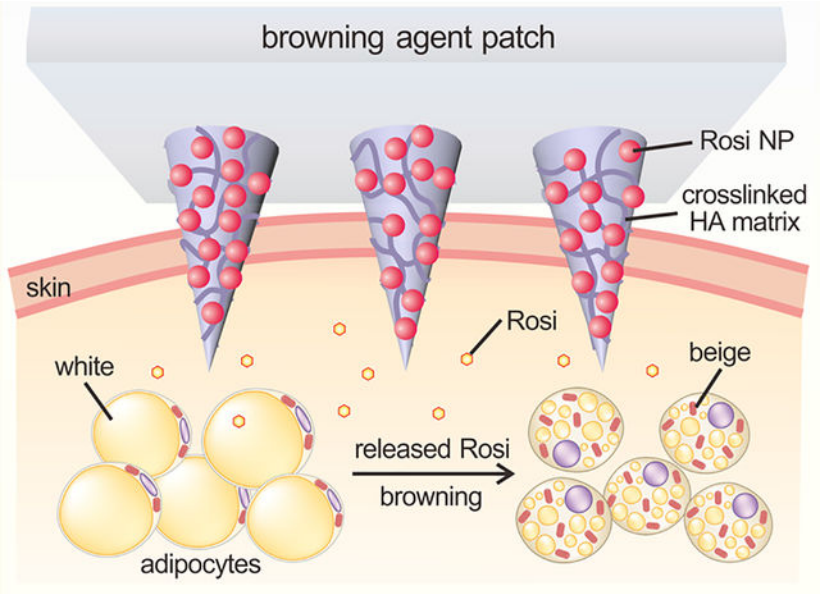

Keywords

drug delivery; microneedle patch; obesity; browning agent; adipose tissue

Obesity has been classified as a disease by the American Medical Association in 2013 and recognized as one of the most serious public health problems in the 21st century associated with rapid global socioeconomic development.[1] Obesity-associated disorders such as type-2 diabetes, cardiovascular diseases, and cancer have become a global threat to human health. Particularly in the United States, more than one-third of the adult population is obese, and the prevalence is going to soar in the next decades.[2] Current treatments toward obesity include restriction of calorie intake by diet programs, promoting energy expenditure through physical exercise, pharmacological therapy, as well as bariatric surgeries and liposuction.[3,4] However, most therapeutics come with undesired side effects on human organs such as gastrointestine, liver, and kidney,[5,6] and surgeries have high risks.[7] Therefore, there is an urgent requirement to exploit effective treatments for obesity.

Recent studies have revealed a crucial role of brown adipose tissue (BAT), a primary heat generation organ, in energy expenditure in mammals.[8,9] It is known that the white adipose tissue (WAT) stores exceeded energy as triglycerides, leading to weight gain; whereas BAT dissipates energy by producing heat through nonshivering thermogenesis, which may facilitate the suppression of obesity.[10] The transformation of WAT into BAT provides an alternative approach for the treatment of obesity and related metabolic disorders, which has garnered increasing attention in the past decade.[11–13] A variety of genes and pathways that regulate adipocyte development have been identified.[4,14] However, numerous browning agents that can promote “browning” on WAT face challenges in clinical application because of undesired side effects on other organs as a result of the broad targeting spectrum.[15–17]

Herein, we report a locally induced browning technology that based on a degradable microneedle (MN) patch consisted of drug-loaded nanoparticles (NPs) and cross-linked matrix (Figure 1). Rosiglitazone (Rosi) or CL 316243 was loaded in the NPs as the model browning agent.[18] The NPs can be further integrated into a microneedle (MN) array based transdermal device for sustained drug delivery into subcutaneous adipose tissue. The MN patch provides a localized, convenient, and painless administration method.[19–22] In a mouse model, we have demonstrated that this MN patch can offer local delivery of browning reagents in a safe and effective manner for inhibition of adipocyte hypertrophy and the consequent improvement of metabolism.

RESULTS AND DISCUSSION

Synthesis and Characterization of Rosi-Loaded NPs.

The degradable NPs were prepared using an acid-sensitive dextran derivative by a double-emulsion method.[23] The acid-sensitive dextran was synthesized through conjugation with ethoxypropene via an acid-catalyzed reaction, which rendered the derived dextran (*m*-dextran) with 89% substitution of hydroxyl to pendant acetals (Figure S1). Rosi, an agonist of peroxisome proliferator-activated receptor gamma (PPARγ), has been reported to stimulate adipose tissue transformation by upregulating uncoupling proteins, VEGF, and angiopoietin-like4.[24,25] We encapsulated Rosi in the dextran NPs for WAT browning. Two enzymes, glucose oxidase (GOx) and catalase (CAT), were introduced into the system to generate acidic environment under the physiological glucose concentration. The GOx is able to convert glucose to gluconic acid to decrease the local pH;[26] while the CAT helps consume undesired hydrogen peroxide produced during the GOx-medicated enzymatic reaction.[27,28] The resulting NPs had spherical shapes with monodisperse distribution as shown in the scanning electron microscopy (SEM) image (Figure 2e). The hydrodynamic particle size was around 250 nm as determined by dynamic light scattering (DLS) (Figure 2a). The NPs had a loading capacity of 5.2 wt %, and encapsulated efficiency was around 55%. To monitor the release kinetics of Rosi, the NPs were incubated in the PBS buffer containing glucose at a normoglycemic level (100 mg/dL) in the human body. Then, the NPs gradually disassociated in the enzyme-induced acidic environment, triggering the encapsulated drug release (Figure 2b). The NPs with GOx gradually degraded in 3 days according to the reduction of the UV absorbance at 400 nm (Figure 2d) and subsequently released the embedded drug (Figure 2c, e). On the contrary, insignificant drug was collected from the NPs without GOx.

To validate the efficiency of Rosi NPs, we employed *in vitro* adipocyte model PgKO-PPARγ1 in which the reconstitution of a shorter form of PPARγ (γ1) in *Pparg*$^{-/-}$ mouse embryonic fibroblast (MEF) rescues adipocyte differentiation only in the presence of exogenous thiazolidinedione class of ligand (*e.g.*, Rosi).[29] Rosi NPs were as efficient as nude Rosi to induce adipocyte formation, evidenced by the same induction of lipid droplet-binding protein genes *aP2* and *Perilipin* (Figure 2f), both of which are canonical PPARγ target genes. Besides the adipogenic potential, we also compared the browning capacity of Rosi NPs. In fully differentiated 3T3-L1 adipocytes, Rosi NPs behaved the same as nude Rosi to up-regulate brown adipocyte markers *Elovl3* and *Cidea* as well as to repress white

adipocyte genes *Resistin* and *Adipsin* (Figure 2g).[30] Therefore, our nanoparticalization strategy is able to sustain a constant release of Rosi at the physiological level of glucose without affecting its efficiency.

Fabrication and Characterization of Browning Agent MN-Array Patch.

The NPs were further embedded into a polymeric MN-array patch for local delivery of browning reagents. Briefly, the NPs were first loaded into the tip region of a silicone MN-mold by centrifugation, following with the addition of base solution. Methacrylated hyaluronic acid (*m*-HA) was selected as the base material, considering its good biocompatibility and mechanical property.[31,32] The *m*-HA base solution mixed with the cross-linker *N,N′*-methylenebis-(acrylamide) (MBA) and a photoinitiator was further cross-linked through polymerization reaction upon exposure to UV light (365 nm, 9 mW/cm^2 for 30s). The cross-linked HA-based matrix can enhance the stiffness of the MNs (Figure S2) for efficient penetration through the skin[19,33] as well as enable sustained release of drug from the MN tips, which helps maintain local constitutive high drug concentrations in adipose tissues. The MN-array contains 121 needles in a 7 × 7 mm^2 patch with a center-to-center interval of 600 μm. Each MN was of a conical shape, with 300 μm in diameter at the base and 800 μm in height (Figure 2h). The zoomed SEM image confirmed the distribution of NPs in the tip (Figure 2i).

In Vivo Studies of the MNs on Lean Mice.

We next examined the *in vivo* browning efficacy of the system in a mouse model. In addition to Rosi, we employed CL 316243, a β3-adrenergic receptor agonist, in the dextran NPs and loaded in the MNs. CL 316243 is a potent thermogenic activator but through a distinct mechanism from Rosi.[34–36] It stimulates G protein $G_{\alpha s}$ to activate adenylate cyclase, and consequently causes the accumulation of cyclic adenosine monophosphate (cAMP), which leads to thermogenesis and lipolysis.[37,38] By including this distinctive browning agent, we would like to evaluate the applicability of our system to other drugs. Specifically, wide-type C57BJ/6 mice were randomly divided into three groups (n = 6) and treated with the empty vehicle MN (EV) made of only cross-linked *m*-HA, the HA MN encapsulating Rosi NPs (10 mg/kg bw) (Rosi), and the CL 316243 NP-loaded MN (1 mg/kg bw) (CL) at inguinal WAT. The MNs could penetrate the mouse skin at the inguinal site efficiently, as evidenced by the trypan blue staining of the MN-treated tissue (Figure 2k). It allowed the tips of MN expose to the inguinal adipose tissue and successfully delivered model drugs into the adipocytes, as evidenced in the fluorescence microscope image (Figure S3). *In vivo* fluorescence imaging of the Cy5.5-labeled nondegradable NPs without GOx loaded MNs verified that the NPs were able to be well restricted in the treated skin region during the whole treatment (Figure S4). The SEM of the MN revealed the collapsed tips after application, further verifying the complete release of drug (Figure 2j). The *in vivo* sustained release within 3 days was also confirmed by *in vivo* fluorescence imaging. Compared to the rapid release of free Cy5.5-loaded MN patch, the degradable NPs-loaded patch showed excellent sustained release capability (Figure S5). The mice were treated with MN patches every 3 days. Six days post-treatment, the mice were sacrificed and the inguinal adipose tissues were collected for histological and gene analysis. The hematoxylin and eosin (H&E) staining of inguinal WAT depicted shrinkage of unilocular white adipocytes and appearance of paucilocular

adipocytes, the typical morphology of beige adipocyte, in Rosi MN and CL 316243 MN treated groups, particularly the latter (Figure 3a). Gene expression analyses further support the browning transformation of the inguinal WAT by MN delivery of browning agents (Figure 3b). The representative brown adipocyte genes including *Ucp1, Dio2, Elovl3, Cidea, Pgc-1α, Cox7a1*, and *Cox8b*, which are involved in mitochondrial activity and lipid utilization, were up-regulated in both groups, while the inflammatory gene *IL-6* was tended to be down-regulated. Interestingly, pan-adipocyte marker *Adiponectin* was not affected, suggesting a selective regulation on browning. Notably, the canonical PPARγ target *aP2* was up-regulated by Rosi MN but not CL 316243 MN, buttressing their distinct browning mechanisms.

After establishing the feasibility of our MN approach to induce browning *in vivo*, we set out to test whether the browning effects of Rosi MN and CL 316243 MN, if genuine, are lasting and physiologically significant. To this end, we exposed Rosi MN- or CL 316243 MN-treated mice together with vehicle MN-treated control mice to indirect calorimetric analysis to measure their systemic metabolic response. All three groups of mice lost weight during the experiment due to the stress from single-housing, but the CL 316243 MN group tended to lose more (Figure 4a).[39–41] Their higher body weight loss arose from reduced fat mass particularly visceral epididymal WAT (eWAT) (Figure 4b,c). The changes in energy homeostasis were merely caused by energy expenditure since neither Rosi MN nor CL 316243 affected calorie intake (Figure 4d). Strikingly, both treatments increased oxygen consumption (Figure 4f) as an outcome from induced browning (Figure 3). Unlike CL 316243 MN, Rosi MN reduced the locomotor activity during the dark cycle when mice are more active (Figure 4e), in line with their distinct browning mechanisms. Furthermore, both Rosi and CL 316243 decreased respiration exchange ratio (RER) (Figure 4g), reflected by released CO_2/consumed O_2, indicating their preference of fatty acid utilization after browning since only 75% oxygen is needed to fully oxidize carbohydrates compared to fatty acids (3:4 ratio). Taken together, our calorimetric studies completely supported the notion that MN delivery of Rosi or CL 316243 browning reagents is an efficient way to induce browning and improve metabolism.

In Vivo Studies of the MNs on Diet-Induced Obese Mice.

Encouraged by these striking physiological effects of our MN browning agent patches, we further evaluated their therapeutic potentials in obese mice. In high-fat diet (HFD)-induced obese C57BL/6 mice, we applied the MN browning agent patch to one side inguinal region (Rosi and CL) and the empty HA MN to the other side as vehicle control (EV-R and EV-C) (Figure 5a). For the control mice, both sides were treated with empty HA MN (EV). Rosi is a potent insulin sensitizer but also causes weight gain. Surprisingly, MN delivery of Rosi also prevented weight gain as CL 316243 MN did, resulting in a ~15% inhibition at the end of this four-week treatment (Figure 5b). Both Rosi MN and CL 316243 MN efficiently improved glucose clearance rate after injecting the mice a bolus of glucose, named intraperitoneal glucose tolerance testing (IPGTT) (Figure 5c), and decreased fasting blood glucose levels (the diagnostic indicator of diabetes) from 140 mg/dL in control mice to ~110 mg/dL (Figure 5d), indicating an improvement of insulin sensitivity. Intriguingly, this improvement is caused by browning rather than by the insulin sensitizing function of Rosi

itself since CL 316243 showed the same effect. As a consequence of increased browning and lipid utilization as we see in Figure 4, we observed a ~30% reduction of eWAT (Figure 5e) but not in the classic interscapular BAT (Figure 5f). More importantly, the MN delivery of browning agents reduced inguinal fat pad locally. The sizes of treated sides, either by Rosi MN or CL 316243 MN, were reduced compared to untreated side (EV-R or EV-C) (Figure 5g, h). Supportively, the H&E stained sections revealed apparently smaller adipocytes in inguinal WAT only in the groups administered with drug-containing patches, but no obvious browning observed on the other site that injected with empty patches (Figure 5i). Brown adipocyte genes were more highly induced in the treated side, particularly by Rosi MN (Figure 5j), indicating a restricted browning effect of MN patches. As an indicator of improved adipose health, *Adiponectin* was up-regulated in both Rosi MN and CL 316243 MN treated side (Figure 5j). Whereas PPARγ downstream target *aP2* was only induced by MN Rosi (Figure 5j), further supporting a local effect of MN patch. Additionally, as presented in the H&E stained histological images of the mouse skin surrounding the MN-treated area after one-month administration, there were insignificant lesions in the skin, indicating excellent biocompatibility of the MN patches (Figure S6).

CONCLUSIONS

In conclusion, we developed a technique based on a NPs integrated microneedle patch that enables local browning of WAT. The degradable NPs released browning agents into the subcutaneous region in the presence of glucose and promoted the transformation of WAT toward the brown-like adipose tissue. More importantly, MNs restricted the browning reagents in the treated region and thus are expected to minimize potential side effects of browning reagents on other organs if administrated orally or intravenously. Our *in vivo* studies further demonstrated systemically increase of energy expenditure and fatty acid oxidation, effective body weight control in diet-induced obese mice, as well as improved insulin sensitivity. Taken together, our work provides an alternative strategy in applying drugs through MN as potential therapeutics for the clinical treatment of obesity and its comorbidities such as type-2 diabetes.[42,43]

METHODS

Materials.

All chemicals were purchased from Sigma-Aldrich unless otherwise specified and were used as received. Rosiglitazone was ordered from Abcam (Cambridge, MA). CL 316243 was purchased from Cayman Chemical (Ann Arbor, MI). The deionized water was prepared by a Millipore NanoPure purification system (resistivity higher than 18.2 MΩ cm^{-1}).

Preparation of Rosiglitazone-Loaded Dextran Nanoparticles.

Dextran nanoparticles were prepared by an improved double-emulsion method as reported previously.[23] Briefly, 5 mL of dichloromethane (DCM) containing 200 mg of *m*-dextran and 20 mg of Rosi was emulsified with 0.5 mL of aqueous solution containing 3.5 mg of enzymes (weight ratio of glucose oxidase to catalase 4:1) by sonication for 45 cycles (1 s each with a duty of 40%). The resulting primary solution was further poured into 25 mL of

1% alginate aqueous solution (M_v = 1.6 × 10^5 Da) for another 45-cycle sonication. The double emulsion was immediately transferred into 150 mL of 0.2% alginate and stirred at room temperature for 2 h to evaporate DCM. Afterward, nanoparticles were collected by centrifugation at 10000 rpm and washed with distilled water three times. The loading capacity (LC) and encapsulation efficiency (EE) of Rosi were determined by measuring the UV−vis absorption of the released Rosi from nanoparticles using a Nanodrop 2000C spectrometer (Thermo Scientific) at absorbance 317 nm. LC and EE were calculated as LC = B/C, EE = B/A, where A was expected encapsulated amount of Rosi, B was the encapsulated amount of Rosi, and C was the total weight of the particles. Particle size and polydispersity intensity were measured by dynamic light scattering (DLS). The zeta potential of the NPs was determined by their electrophoretic mobility using the same instrument after appropriate dilution in DI water. Measurements were made in triplicate at room temperature. NPs morphology was investigated by a FEI Verios 460L field-emission scanning electron microscope (FESEM).

In vitro Release Studies.

The *in vitro* release profile of Rosi from dextran nanoparticles was evaluated through incubation of nanoparticles in 1 mL of PBS buffer (NaCl, 137 mM; KCl, 2.7 mM; Na_2HPO_4, 10 mM; KH_2PO_4, 2 mM; pH 7.4) at 37 °C on an orbital shaker, to which 100 mg/dL glucose was added to reach normoglycemic level in human body. At predetermined time points, the sample was centrifuged (10000 rpm, 1 min) and 10 μL of the supernatant was taken out for analysis by measuring the UV−vis absorbance at 317 nm using a Nanodrop 2000C spectrometer.

Fabrication of Browning Agent MN Patch.

All the MNs in this study were fabricated using the uniform silicone molds from Blueacre Technology, Ltd. Each needle had a 300 μm by 300 μm round base tapering to a height of 800 μm. The needles were arranged in an 11 × 11 array with 600 μm tip-to-tip spacing. To fabricate a nanoparticle-loaded microneedle, the prepared nanoparticle suspension was first deposited by pipet onto the MN mold surface (30 μL/array). Then molds were placed under vacuum (600 mmHg) for 5 min to allow the solution filled the MN cavities. Afterward, the covered molds were centrifuged using a Hettich Universal 32R centrifuge for 10 min at 2000 rpm. Finally, 3 mL of premixed *N,N*′-methylenebis(acrylamide) (MBA, w/v 2%), photoinitiator (Irgacure 2959, w/v 0.5%), and *m*-HA solution (w/v: 4%) was added into the prepared micromold reservoir and allowed to dry at 20 °C under vacuum desiccator. *m*-HA was synthesized following the previous reported method.[44] After complete desiccation, the MN patch was carefully detached from the silicone mold and underwent the cross-linking polymerization via UV irradiation (wavelength: 365 nm at an intensity of 9 mW/cm^2) for 30 s. The resulting MN-array patches were stored in a sealed six well container for later study. The morphology of the MNs was characterized via a FEI Verios 460L field-emission scanning electron microscope (FESEM).

In vivo Browning Studies in Lean Mice.

Eight-week old male C57BL/6 mice ordered from Charles River (Raleigh, NC) or the Jackson Laboratory were used. The animal study protocols were approved by the

Institutional Animal Care and Use Committee at North Carolina State University and University of North Carolina at Chapel Hill or by the Columbia University Animal Care and Utilization Committee. Mice were caged at 22 ± 1 °C with free access to water and regular chow diet on a 12 h light/dark cycle. Mice were given least 1 week adaption before experiments. Three groups of animals ($n = 6$) were treated with empty HA MN patch (EV), Rosi NP-loaded MN patch (10 mg/kg) (Rosi), or CL316243 NP-loaded MN patch (1 mg/kg) (CL), respectively, on inguinal regions every 3 days. For indirect calorimetric studies, mice were subjected to the Comprehensive Lab Animal Monitoring System (CLAMS). Metabolic activities were monitored during the treatment, including oxygen consumption, food intake, locomotor activity, and body weight. Six days post administration, animals were sacrificed and inguinal adipose tissues were collected for histological and RNA analysis. Interscapular BAT and epididymal WAT were weighted.

Browning MN Patch Treatments on Diet Induced Obesity mice.

Male C57BL/6 mice were fed on a HFD (60% kcal from fat) for 8 weeks to induce obesity and insulin resistance. Three groups with five mice for each group were treated with empty HA, Rosi (10 mg/kg), or CL316243 (1 mg/kg) through a transdermal patch on one side of the inguinal areas under isoflurane anesthesia. The other side of inguinal tissue of each mouse was administrated with an empty HA microneedle patch. The patch was changed every 3 days for 4 weeks. Body weight was monitored during the treatment period. The glucose tolerance test was performed in mice 3-weeks post-treatment. The mice were fasted for 16 h (overnight) before glucose administration. The mice were intraperitoneal injected with glucose at 2 g/kg diluted in PBS, and blood glucose levels were monitored over time. At the end of 4-weeks MN treatment, the animals were euthanized by CO_2 asphyxiation, and adipose tissues (inguinal WAT, epididymal WAT, and interscapular BAT) were collected for analyses. The skin tissues around the treated areas were also collected for biocompatibility evaluation of MN patches.

Supplementary Material

Refer to Web version on PubMed Central for supplementary material.

ACKNOWLEDGMENTS

This work was supported by a grant from the NC TraCS, NIH's Clinical and Translational Science Awards (CTSA, NIH Grant No. 1UL1TR001111) at UNC−CH, and NIH Grant Nos. R00DK97455 (L.Q.) and P30DK063608 (L.Q.). We acknowledge the use of the Analytical Instrumentation Facility (AIF) at NC State, which is supported by the State of North Carolina and the National Science Foundation (NSF). The strain tests were made using a DTS delaminator supported by the UNC Research Opportunity Initiative. All animals were treated in accordance with the Guide for Care and Use of Laboratory Animals, approved by the Institutional Animal Care and Use Committee (IACUC) of University of North Carolina at Chapel Hill and North Carolina State University, or by the Columbia University Animal Care and Utilization Committee.

REFERENCES

(1). World Health Organization. Obesity and Overweight. Fact Sheet No, 311, 2015, http://www.who.int/mediacentre/factsheets/fs311/en/.

(2). Ogden CL; Carroll MD; Fryar CD; Flegal KM Prevalence of Obesity Among Adults and Youth: United States, 2011− 2014. NCHS Data Brief 2015, 219, 1–8.

(3). Friedman JM Obesity: Causes and Control of Excess Body Fat. Nature 2009, 459, 340–342. [PubMed: 19458707]

(4). Heymsfield SB; Wadden TA Mechanisms, Pathophysiology, and Management of Obesity. N. Engl. J. Med 2017, 376, 254–266. [PubMed: 28099824]

(5). Rucker D; Padwal R; Li SK; Curioni C; Lau DC Long Term Pharmacotherapy for Obesity and Overweight: Updated Meta-Analysis. BMJ. 2007, 335, 1194–9. [PubMed: 18006966]

(6). Dietrich MO; Horvath TL Limitations in Anti-Obesity Drug Development: the Critical Role of Hunger-Promoting Neurons. Nat. Rev. Drug Discovery 2012, 11, 675–691. [PubMed: 22858652]

(7). Chang S-H; Stoll CR; Song J; Varela JE; Eagon CJ; Colditz GA The Effectiveness and Risks of Bariatric Surgery: an Updated Systematic Review and Meta-Analysis, 2003−2012. JAMA Surg. 2014, 149, 275–287. [PubMed: 24352617]

(8). Wu J; Cohen P; Spiegelman BM Adaptive Thermogenesis in Adipocytes: Is Beige the New Brown? Genes Dev. 2013, 27, 234–250. [PubMed: 23388824]

(9). Au-Yong IT; Thorn N; Ganatra R; Perkins AC; Symonds ME Brown Adipose Tissue and Seasonal Variation in Humans. Diabetes 2009, 58, 2583–2587. [PubMed: 19696186]

(10). Kajimura S; Spiegelman BM; Seale P Brown and Beige Fat: Physiological Roles Beyond Heat Generation. Cell Metab. 2015, 22, 546–559. [PubMed: 26445512]

(11). Harms M; Seale P Brown and Beige Fat: Development, Function and Therapeutic Potential. Nat. Med 2013, 19, 1252–1263. [PubMed: 24100998]

(12). Bartelt A; Heeren J Adipose Tissue Browning and Metabolic Health. Nat. Rev. Endocrinol 2014, 10, 24–36. [PubMed: 24146030]

(13). Xue Y; Xu X; Zhang X-Q; Farokhzad OC; Langer R Preventing Diet-Induced Obesity in Mice by Adipose Tissue Transformation and Angiogenesis Using Targeted Nanoparticles. Proc. Natl. Acad. Sci. U. S. A 2016, 113, 5552–5557. [PubMed: 27140638]

(14). Bonet ML; Oliver P; Palou A Pharmacological and Nutritional Agents Promoting Browning of White Adipose Tissue. Biochim. Biophys. Acta, Mol. Cell Biol. Lipids 2013, 1831, 969–985.

(15). Clapham JC; Arch JR; Tadayyon M Anti-Obesity Drugs: a Critical Review of Current Therapies and Future Opportunities. Pharmacol. Ther 2001, 89, 81–121. [PubMed: 11316515]

(16). Whittle A; Relat-Pardo J; Vidal-Puig A Pharmacological Strategies for Targeting BAT Thermogenesis. Trends Pharmacol. Sci 2013, 34, 347–355. [PubMed: 23648356]

(17). Colman E; Golden J; Roberts M; Egan A; Weaver J; Rosebraugh C The FDA's Assessment of Two Drugs for Chronic Weight Management. N. Engl. J. Med 2012, 367, 1577–1579. [PubMed: 23050510]

(18). Nedergaard J; Cannon B The Browning of White Adipose Tissue: Some Burning Issues. Cell Metab. 2014, 20, 396–407. [PubMed: 25127354]

(19). Prausnitz MR; Langer R Transdermal Drug Delivery. Nat. Biotechnol 2008, 26, 1261–1268. [PubMed: 18997767]

(20). Cai X; Jia X; Gao W; Zhang K; Ma M; Wang S; Zheng Y; Shi J; Chen H A Versatile Nanotheranostic Agent for Efficient Dual-Mode Imaging Guided Synergistic Chemo-Thermal Tumor Therapy. Adv. Funct. Mater 2015, 25, 2520–2529.

(21). Ye Y; Yu J; Wang C; Nguyen NY; Walker GM; Buse JB; Gu Z Microneedles Integrated with Pancreatic Cells and Synthetic Glucose-Signal Amplifiers for Smart Insulin Delivery. Adv. Mater 2016, 28, 3115–3121. [PubMed: 26928976]

(22). Wang C; Ye Y; Hochu GM; Sadeghifar H; Gu Z Enhanced Cancer Immunotherapy by Microneedle Patch-Assisted Delivery of Anti-PD1 Antibody. Nano Lett. 2016, 16, 2334–2340. [PubMed: 26999507]

(23). Gu Z; Aimetti AA; Wang Q; Dang TT; Zhang Y; Veiseh O; Cheng H; Langer RS; Anderson DG Injectable Nano-Network for Glucose-Mediated Insulin Delivery. ACS Nano 2013, 7, 4194–4201. [PubMed: 23638642]

(24). Bakopanos E; Silva JE Thiazolidinediones Inhibit the Expression of Beta3-Adrenergic Receptors at a Transcriptional Level. Diabetes 2000, 49, 2108–2115. [PubMed: 11118014]

(25). Cipolletta D; Feuerer M; Li A; Kamei N; Lee J; Shoelson SE; Benoist C; Mathis D PPARγ is a Major Driver of the Accumulation and Phenotype of Adipose Tissue Treg Cells. Nature 2012, 486, 549–553. [PubMed: 22722857]

(26). Mo R; Jiang T; Di J; Tai W; Gu Z Emerging Micro-and Nanotechnology Based Synthetic Approaches for Insulin Delivery. Chem. Soc. Rev 2014, 43, 3595–3629. [PubMed: 24626293]

(27). Yu J; Zhang Y; Bomba H; Gu Z Stimuli-Responsive Delivery of Therapeutics for Diabetes Treatment. Bioeng. Transl. Med 2016, 1, 323–337. [PubMed: 29147685]

(28). Zhang Y; Yu J; Shen Q; Gu Z Glucose-Responsive Synthetic Closed-Loop Insulin Delivery Systems. Prog. Chem 2015, 27, 11–26.

(29). Li D; Zhang F; Zhang X; Xue C; Namwanje M; Fan L; Reilly MP; Hu F; Qiang L Distinct Functions of PPARγ Isoforms in Regulating Adipocyte Plasticity. Biochem. Biophys. Res. Commun 2016, 481, 132–138. [PubMed: 27818196]

(30). Vernochet C; Peres SB; Davis KE; McDonald ME; Qiang L; Wang H; Scherer PE; Farmer SR C/EBPα and the Corepressors CtBP1 and CtBP2 Regulate Repression of Select Visceral White Adipose Genes During Induction of the Brown Phenotype in White Adipocytes by Peroxisome Proliferator-Activated Receptor γ Agonists. Mol. Cell. Biol 2009, 29, 4714–4728. [PubMed: 19564408]

(31). Kogan G;Šoltes L; Stern R; Gemeiner P Hyaluronic Acid: a Natural Biopolymer with a Broad Range of Biomedical and Industrial Applications. Biotechnol. Lett 2007, 29, 17–25. [PubMed: 17091377]

(32). Yu J; Zhang Y; Ye Y; DiSanto R; Sun W; Ranson D; Ligler FS; Buse JB; Gu Z Microneedle-Array Patches Loaded with Hypoxia-Sensitive Vesicles Provide Fast Glucose-Responsive Insulin Delivery. Proc. Natl. Acad. Sci. U. S. A 2015, 112, 8260–8265. [PubMed: 26100900]

(33). Zhang Y; Yu J; Wang J; Hanne NJ; Cui Z; Qian C; Wang C; Xin H; Cole JH; Gallippi CM Thrombin-Responsive Transcutaneous Patch for Auto-Anticoagulant Regulation. Adv. Mater 2017, 29, 1604043.

(34). Lowell BB; Flier JS Brown Adipose Tissue, β3-Adrenergic Receptors, and Obesity. Annu. Rev. Med 1997, 48, 307–316. [PubMed: 9046964]

(35). Weyer C; Gautier J; Danforth E Jr Development of Beta 3-Adrenoceptor Agonists for the Treatment of Obesity and Diabetes An Update. Diabetes Metab. 1999, 25, 11–21.

(36). Weyer C; de Souza CJ Development of β3-Adrenoceptor Agonists as Antiobesity and Antidiabetes Drugs in Humans: Current Status and Future Prospects. Drug Dev. Res 2000, 51, 80–93.

(37). Klein J; Fasshauer M; Ito M; Lowell BB; Benito M; Kahn CR β3-Adrenergic Stimulation Differentially Inhibits Insulin Signaling and Decreases Insulin-Induced Glucose Uptake in Brown Adipocytes. J. Biol. Chem 1999, 274, 34795–34802. [PubMed: 10574950]

(38). Yu S; Gavrilova O; Chen H; Lee R; Liu J; Pacak K; Parlow A; Quon MJ; Reitman ML; Weinstein LS Paternal versus Maternal Transmission of a Stimulatory G-Protein α Subunit Knockout Produces Opposite Effects on Energy Metabolism. J. Clin. Invest 2000, 105, 615–623. [PubMed: 10712433]

(39). Voikar V; Polus A; Vasar E; Rauvala H Long-Term Individual Housing in C57BL/6J and DBA/2 Mice: Assessment of Behavioral Consequences. Genes, Brain Behav. 2005, 4, 240–252. [PubMed: 15924556]

(40). Nagy TR; Krzywanski D; Li J; Meleth S; Desmond R Effect of Group vs. Single Housing on Phenotypic Variance in C57BL/6J Mice. Obes. Res 2002, 10, 412–415. [PubMed: 12006642]

(41). Kalliokoski O; Jacobsen KR; Darusman HS; Henriksen T; Weimann A; Poulsen HE; Hau J; Abelson KS Mice Do Not Habituate to Metabolism Cage Housing−a Three Week Study of Male BALB/c Mice. PLoS One 2013, 8, e58460. [PubMed: 23505511]

(42). Lu Y; Aimetti AA; Langer R; Gu Z Bioresponsive Materials. Nat. Rev. Mater 2016, 2, 16075.

(43). Sun W; Hu Q; Ji W; Wright G; Gu Z Leveraging Physiology for Precision Drug Delivery. Physiol. Rev 2017, 97, 189–225.

(44). Jiang T; Mo R; Bellotti A; Zhou J; Gu Z Gel−Liposome-Mediated Co-Delivery of Anticancer Membrane-Associated Proteins and Small-Molecule Drugs for Enhanced Therapeutic Efficacy. Adv. Funct. Mater 2014, 24, 2295–2304.

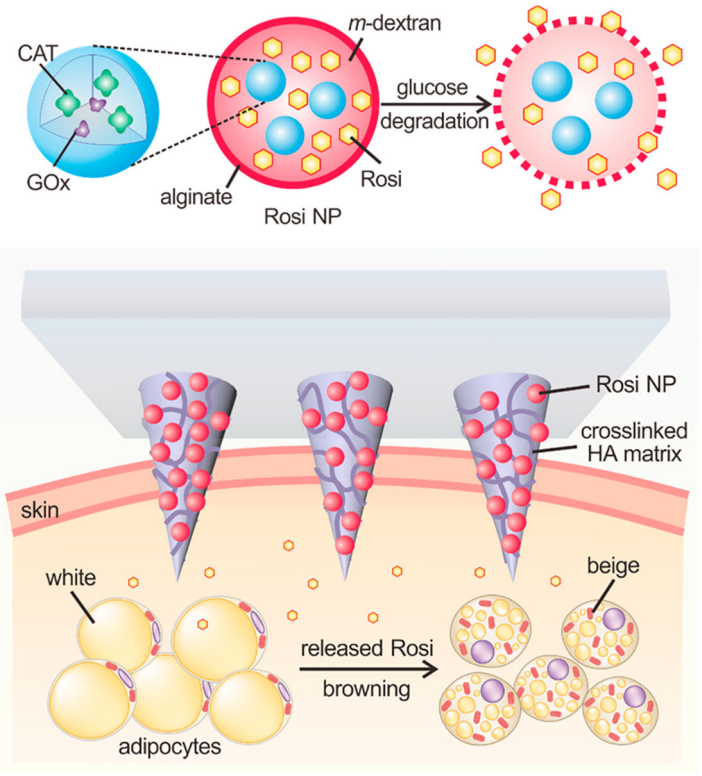

Figure 1.

Schematic illustration of the browning reagents-loaded transcutaneous MN patch. Nanoparticles (NPs) encapsulating rosiglitazone (Rosi), glucose oxidase (GOx), and catalase (CAT) are prepared from pH-sensitive acetal-modified dextran and coated with alginate. NPs are further loaded into the microneedle-array patch made of cross-linked hyaluronic acid (HA) matrix for the brown remodeling of the white fat.

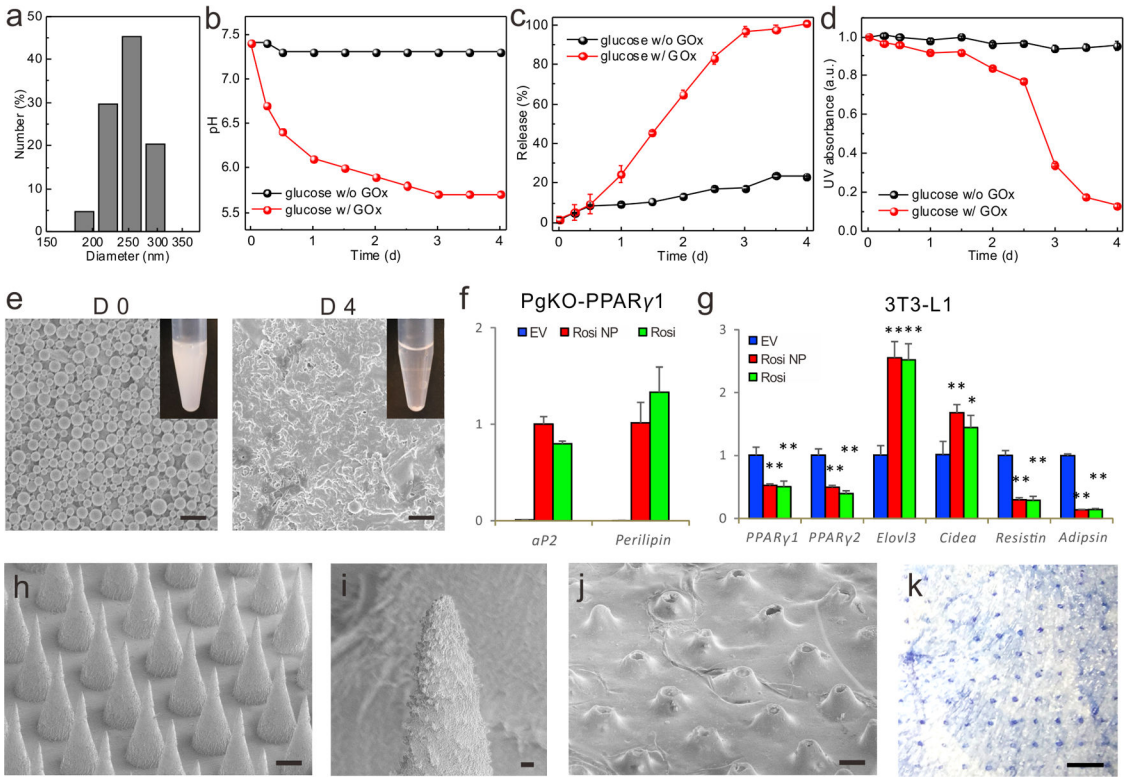

Figure 2.

Fabrication and characterization of browning reagent microneedles. (a) The average hydrodynamic sizes of Rosi NPs determined by DLS. (b) Relevant pH changes of dextran NPs with or without GOx in PBS buffer in the presence of 100 mg/dL glucose. ($n = 3$) (c) *In vitro* accumulated Rosi release from the acid-degradable dextran NPs (w/or w/o GOx) in PBS buffer containing 100 mg/dL glucose at 37 °C. ($n = 3$) (d) UV absorbance of NPs suspensions A_{400} nm. ($n = 3$) (e) SEM images of Rosi NPs incubated in PBS buffer with 100 mg/dL glucose at 37 °C on day 0 and day 4 (scale bar: 2 μm), inset pictures show the transparency change of the NPs suspension. (f) Comparable adipogenesis between Rosi NPs- and Rosi compound-treated PgKO-MEFs as assessed by *aP2* and *Perilipin* gene expression. ($n = 4$). (g) Same level of browning induced by Rosi NPs or Rosi compound in the mature 3T3-L1 white adipocytes. ($n = 4$). (h) SEM image of the MN array (scale bar: 200 μm). (i) Higher magnification of SEM imaging of MN tip confirmed that the MN was loaded with NPs (scale bar: 10 μm). (j) SEM image of MNs 3 days post administration (scale bar: 200 μm). (k) Trypan blue staining image of mouse skin administered with MN patch (scale bar: 1 mm). Error bars indicate standard deviation (SD), two-tailed Student's *t*-test, $*P < 0.05$, $**P < 0.01$.

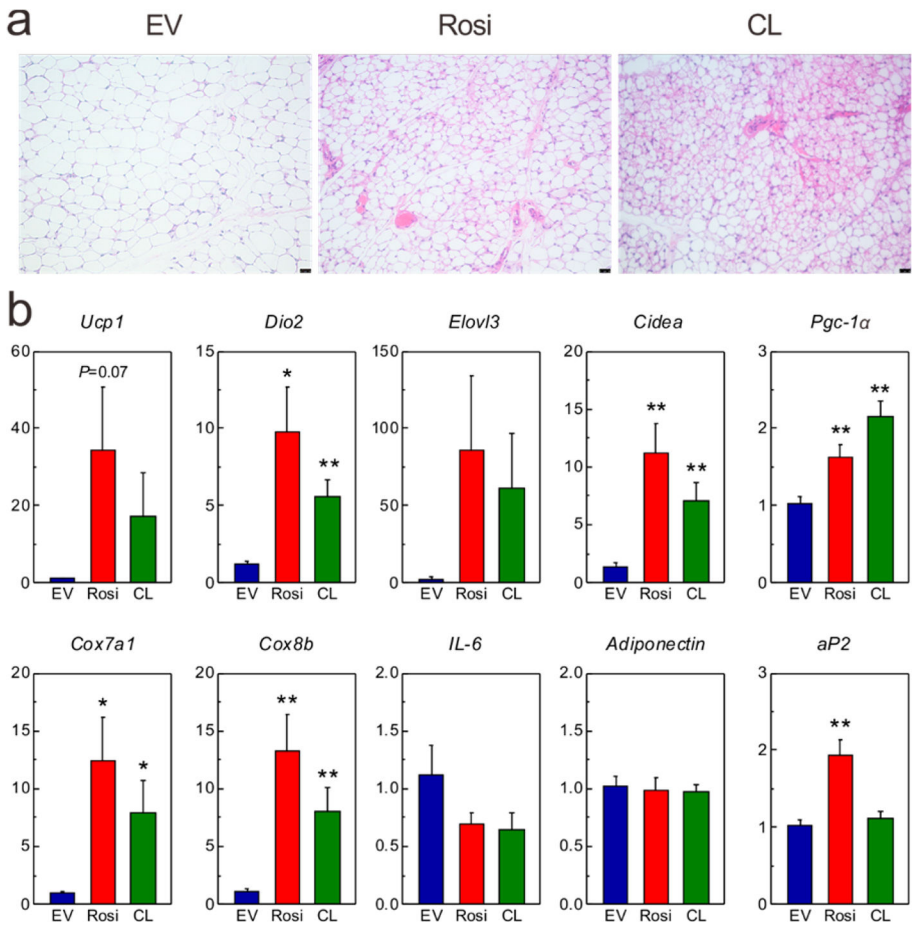

Figure 3.

In vivo browning induction by MN patches in the lean mice. (a) H&E-stained section of the cross-sectional mouse inguinal adipose tissue treated with HA empty MN patch (left), Rosi NP-loaded MN patch (middle), and CL 316243 NP-loaded MN patch (right) (scale bar: 25 μm). (b) Q-PCR analysis of gene expression in inguinal WAT treated with MN patches loaded with HA empty vehicle (EV), Rosi, or CL 316243 (CL). NP-loaded MN patch. Error bars indicate standard error of the mean (SEM), two-tailed Student's *t*-test, $*P < 0.05$, $**P < 0.01$ compared to EV ($n = 6$).

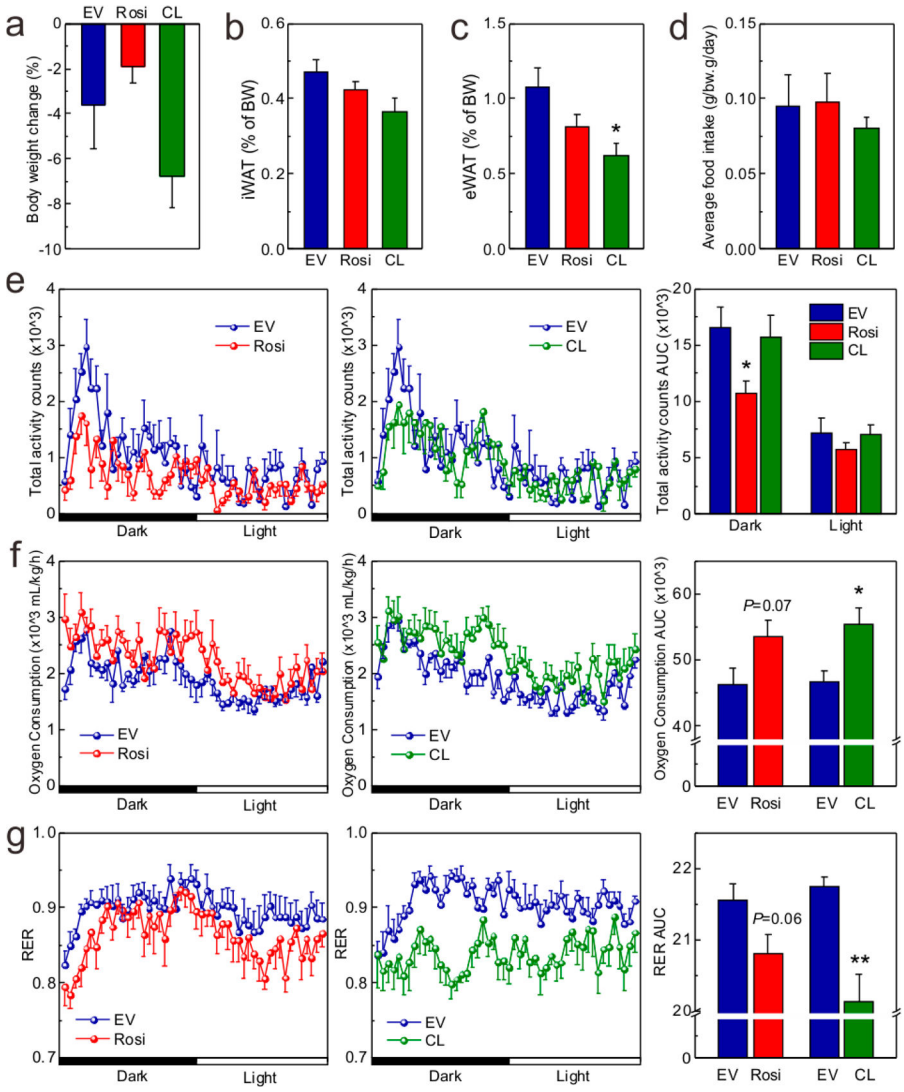

Figure 4.

Indirect calorimetric analysis of healthy mice treated with HA empty MN patch (EV), Rosi NP-loaded MN patch (Rosi), or CL 316243 NP-loaded MN patch (CL). (a) Body weight change after the 6-day treatment. (b) Normalized inguinal fat pad size. (c) Normalized epididymal fat pad size. (d) Average food intake during the treatment. (e) Locomotor activity during one 24-h dark/light cycle. The panel on the right is the area under curve (AUC). (f) Oxygen consumption and AUC. (g) Respiration exchange ratio (RER) and AUC during one dark/light cycle. Error bars indicate SEM, two-tailed Student's *t*-test, $*P < 0.05$, $**P < 0.01$ compared to EV ($n = 6$).

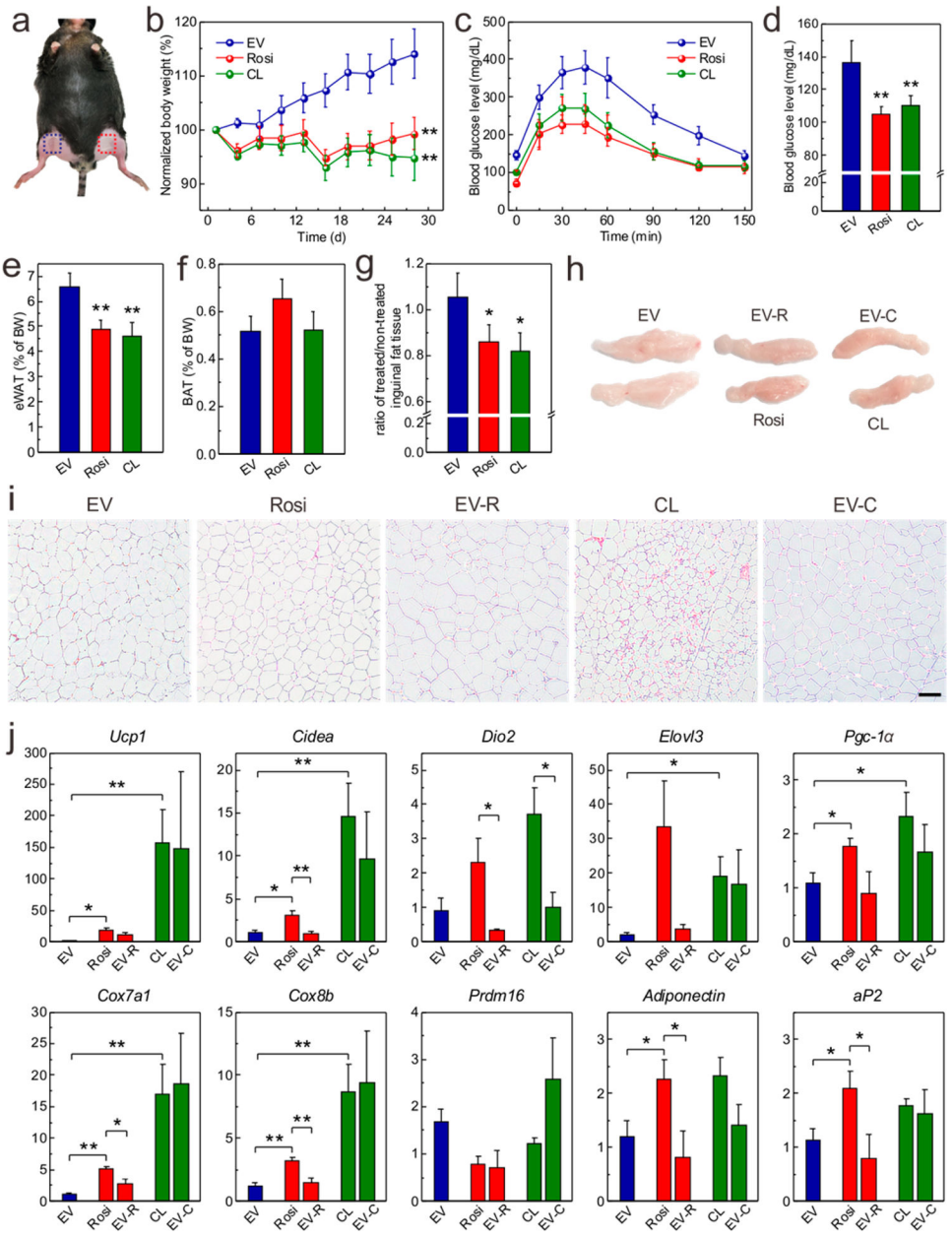

Figure 5.

In vivo antiobesity and antidiabetic effects of MN patches in an HFD-induced obese mouse model. (a) Picture illustrating the mice treated with browning agent patch on one inguinal side (red) and empty vehicle patch on the other side (blue). (b) Normalized body weight of mice without treatment or treated with browning agent patches. (c) IPGTT test in mice 2 weeks post-treatment. (d) Blood glucose levels of mice treated with browning agent patches or empty patches after 16 h fasting. (e) Normalized epididymal fat pad size in mice with different treatments. (f) Normalized weight of interscapular fat pad size in mice with different treatments. (g) Ratio of the treated inguinal fat pad size to untreated side. (h) Photos of two sides of inguinal adipose tissues from obese mice 4-weeks post treatment. (i) H&E staining of inguinal adipose tissues (scale bar: 50 μm). (j) Q-PCR analysis of adipocyte

gene expressions in inguinal tissues. (b−g) Error bars indicate SD, two-tailed Student's *t*-test, $*P < 0.05$, $**P < 0.01$ compared to EV ($n = 5$). (j) Error bars indicate SEM, two-tailed Student's *t*-test, $*P < 0.05$, $**P < 0.01$ compared to EV ($n = 5$).